Korean J. Chem. Eng., 35(7), 1433-1440 (2018)
DOI: 10.1007/s11814-018-0050-8

pISSN: 0256-1115
eISSN: 1975-7220

Comparative study of CHA- and AEI-type zeolytic catalysts for the conversion of chloromethane into light olefins

Yong Hun Shin*, Sungjoon Kweon, Min Bum Park**,†, and Ho-Jeong Chae*,†**

*CO_2 Energy Vector Research Group, Carbon Resources Institute, Korea Research Institute of Chemical Technology, Daejeon 34114, Korea
**Innovation Center for Chemical Engineering, Department of Energy and Chemical Engineering, Incheon National University, Incheon 22012, Korea
(*Received 10 January 2018 • accepted 15 March 2018*)

Abstract−Three pairs of CHA- and AEI-type zeolytic materials with similar crystallite size but with different framework atoms, i.e., silicoaluminophosphate SAPO-34 and SAPO-18, aluminosilicate SSZ-13 and SSZ-39, and titanium-incorporated TiAPSO-34 and TiAPO-18, were prepared and their catalytic activities of chloromethane into light olefins were compared according to the structure types, as well as acidic properties. The AEI-type catalysts were found to have lower ethene/propene ratios, indicating relatively higher propene selectivity, because their *aei*-cage was larger compared to the *cha*-cage. However, all the CHA-type catalysts exhibited better activity and higher selectivity to light olefins. Both H-SAPO-34 and H-TiAPSO-34 showed good catalytic stability over all the reaction times studied here. When compared to H-SAPO-34, however, H-TiAPSO-34 exhibited ca. 20 mol% higher selectivity to ethene and propene, despite a similar total density of acid site. This performance may be due to the higher strength of medium acid sites.

Keywords: AEI, CHA, Chloromethane Conversion, Light Olefins, TiAPSO-34

INTRODUCTION

The transformation of methane to chemical products is a topic of interest in light of the continuing depletion of petroleum crude oil and the increasing availability of plentiful natural gas (like shale gas). Over the past few decades, several direct conversion routes from methane to hydrocarbons have been studied and developed, for example, to methanol, formaldehyde, ethylene, benzene, etc., but the present industrial process still proceeds via syngas (CO and H_2), which can finally be converted to heavier hydrocarbons through Fischer-Tropsch catalysis [1]. Another promising non-syngas indirect method is the transformation of methane to gasoline or light olefins via a halide methane (CH_3X, X=Cl or Br). Methane can be converted to a mono halide methane through the monohalogenation ($CH_4+X_2\rightarrow CH_3X+HX$) or oxyhydrochlorination (OHC) process ($CH_4+HCl+1/2O_2\rightarrow CH_3Cl+H_2O$) and the subsequent conversion of halide methane into hydrocarbons using acid catalysts like H-zeolites [2,3]. The second stage of the halogenated methane transformation greatly resembles the more studied methanol-to-gasoline (MTG) or methanol-to-olefins (MTO) reaction [4]. For example, it has been reported that the chloromethane-to-olefins (CMTO) transformation over H-SAPO-34 (framework type CHA) and H-ZSM-5 (MFI) proceeds through the so-called hydrocarbon pool mechanism, which is now the general consensus for the MTO reaction. The similarly shaped selective catalysis leads to similar product distribution, i.e., high selectivity to light olefins and gasoline range products over H-SAPO-34 and H-ZSM-5, respectively [3,5-8].

However, there are also some obvious distinctions between the two reactions. The CMTO reaction does not generate dimethyl ether, which is usually co-produced in the MTO reaction, but instead generates hydrogen chloride (HCl) as a by-product, which can recycle back to the OHC process [3]. In particular, the most remarkable difference is the lower conversion of chloromethane, as compared to methanol under similar reaction conditions. This may be due to the lower proton affinity of chloromethane and thus a lower rate of transformation [5]. A higher reaction temperature or a stronger and more highly acidic zeolytic catalyst can improve the conversion of chloromethane, but at the same time lead to faster catalyst deactivation. For these reasons, it is necessary to explore how diverse zeolytic catalysts improve the chloromethane conversion and/or selectivity to light olefins. CMTO reactions carried out over zeolytic catalysts, H-ZSM-5 [9-12] and H-SAPO-34 [5-8,13-20] have already been widely reported. Some modifications to the two catalysts have resulted in a further improvement in activity and selectivity [9,10,15]. Some other structural types of zeolites and SAPO materials, for example, beta (*BEA), mordenite (MOR), Y (FAU), MCM-22 (MWW), ZSM-22 (TON), ZSM-34 (OFF/ERI), SAPO-5 (AFI), and SAPO-18 (AEI), have also been studied for this reaction, and it was reported that the conversion and product distribution differed depending on the porous structure and acidity of the catalysts [10,21-25].

Among the wide number of MTO works, many studies have been performed over H-ZSM-5 and H-SAPO-34, with excellent performance. Besides these two most famous catalysts, recently, aluminosilicate CHA-type zeolite SSZ-13, and AEI-type zeolite and SAPO

†To whom correspondence should be addressed.
E-mail: mbpark@inu.ac.kr, hjchae@krict.re.kr

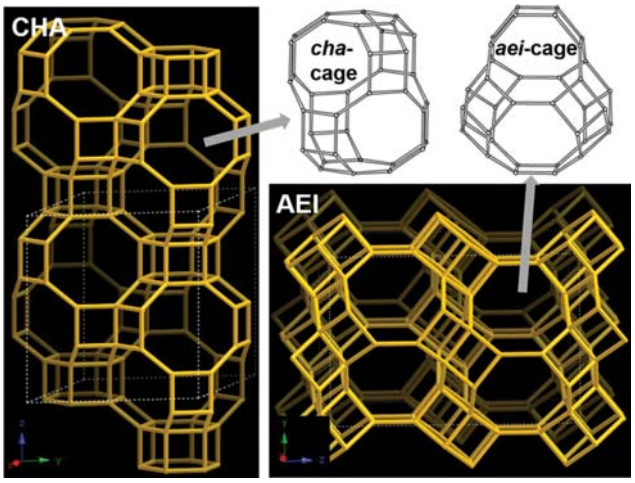

Fig. 1. CHA (left) and AEI (right) structures and their cavities. Adapted from ref. 31.

materials, SSZ-39 and SAPO-18, respectively, have also been investigated and described as efficient catalysts for the MTO reaction [26-30]. As seen in Fig. 1, both the CHA and AEI structures include double six-ring (*d6r*) units stacked along the *z*-axis. However, unlike the CHA structure, AEI has a lateral shift between the *d6r* units, resulting in a rotation of 180° around the *z*-axis [31]. This small difference results in the two structures having different cage features: the cylindrical 20-hedral [$4^{12}6^{2}8^{6}$] *cha*-cages (ca. 6.7×6.7×10 Å) of CHA are accessible through symmetrical 8-ring (3.8×3.8 Å) windows, while the *aei*-cages of AEI with a similar three-dimensional interconnected channel system, and bound by 8-rings (3.8×3.8 Å) have different pear-shaped cages, which can include spheres up to 7.3 Å, wider at the bottom than the *cha*-cage. In the MTO reaction, when compared to H-SAPO-34 vs H-SAPO-18 or H-SSZ-13 vs H-SSZ-39 with adequate acid site densities, the larger size of the *aei*-cages allows the formation of aromatics of the proper size within the hydrocarbon pool transient state and a relative increase in propene over ethene [28,29]. Despite the similarities between the MTO and CMTO reactions, however, there are very few comparative studies of CHA and AEI-type zeolytic catalysts for the CMTO reaction. One study reported that H-SAPO-18 exhibited better CMTO kinetic behavior (initial conversion, catalyst life time, and product selectivity) than H-SAPO-34 due to its moderate acidity [25].

At the same time, some studies have reported that compared to H-SAPO-34, the metal-incorporated H-MeAPSO-34 catalysts (Me= Ti, Mn, Fe, Co, Zr, etc.) improved both MTO and/or CMTO activity by modifying their density and/or the strength of acid sites [15,17,19,32-34]. Co, Mn, and Fe incorporated H-MeAPSO-34 exhibited improved catalyst life time, and favored ethene and propene selectivity in the CMTO reaction [15,17]. In our previous study, we prepared a series of H-TiAPSO-34 catalysts with nanometer scale crystal size, and controlled titanium content in the zeolytic framework; when the H-TiAPSO-34 catalyst incorporated the proper amount of titanium, it had a positive effect on the MTO activity and stability [34]. Accordingly, in the present contribution, we compared CMTO kinetic behaviors based on the CHA and AEI framework topologies, and the composition of the framework atoms (aluminosilicate, SAPO, and TiAPSO or TiAPO molecular sieves). H-TiAPSO-34 showed the best performance for both the chloromethane conversion and selectivity to light olefins among all the catalysts studied here.

EXPERIMENTAL

1. Catalyst Preparation

All as-made materials were synthesized in Teflon-lined autoclaves according to the procedures described previously (Table 1) [34-37]. The solid products were recovered by filtration or centrifugation, washed repeatedly with distilled water, and dried overnight at room temperature. The SAPO, TiAPSO, and TiAPO samples were converted to proton form by calcining in air at 550 °C for 8 h. Since inorganic Na^{+} was used in their synthesis, aluminosilicate SSZ-13 and SSZ-39 zeolites were first calcined in air at 550 °C for 8 h and then converted to proton form by refluxing twice in 1.0 M NH_4NO_3 solution (1.0 g solid per 100 mL solution) at 80 °C for 8 h followed by calcination at 550 °C for 2 h.

2. Analytical Methods

Powder X-ray diffraction (XRD) patterns were recorded on a Rigaku D/MAX Ultima III diffractometer operated at 40 kV and

Table 1. Synthesis conditions for the CHA- and AEI-type zeolytic materials employed in this study

Material	IZA code	Synthesis mixture composition[a]	T/t (°C/days)	Ref.
SAPO-34	CHA	$2.0TEAOH{\cdot}1.0Al_2O_3{\cdot}1.0P_2O_5{\cdot}0.3SiO_2{\cdot}52H_2O$	175/2	[34]
SSZ-13	CHA	$0.2BTMAOH{\cdot}1.0SiO_2{\cdot}0.033Al_2O_3{\cdot}0.05Na_2O{\cdot}5.0H_2O$	125/7	[35]
TiAPSO-34	CHA	$2.0TEAOH{\cdot}1.0Al_2O_3{\cdot}1.0P_2O_5{\cdot}0.3SiO_2{\cdot}0.1TiO_2{\cdot}52H_2O$	175/2	[34]
SAPO-18	AEI	$1.6DIPEA{\cdot}1.0Al_2O_3{\cdot}0.9P_2O_5{\cdot}0.2SiO_2{\cdot}50H_2O$	160/7[b]	[36]
SSZ-39	AEI	$0.14TMPOH{\cdot}1.0SiO_2{\cdot}0.0167Al_2O_3{\cdot}0.3Na_2O{\cdot}28H_2O$	140/5[b]	[37]
TiAPO-18	AEI	$2.0TEAOH{\cdot}1.0Al_2O_3{\cdot}1.0P_2O_5{\cdot}0.3TiO_2{\cdot}52H_2O$	175/5	[34]

[a]TEAOH, BTMAOH, DIPEA, and TMPOH indicate tetraethylammonium hydroxide (35% aqueous solution, Sachem), benzyltrimethylammonium hydroxide (40% aqueous solution, Aldrich), *N,N*-diisopropylethylamine (99%, Aldrich), and 1,1,3,5-tetramethylpiperidinium hydroxide (homemade), respectively. Fumed silica (Aerosil 200, Degussa), sodium silicate solution (Samchun), aluminum isopropoxide (98%, Aldrich), pseudoboehmite (Catapal B, Vista), and Y zeolites (CBV-500 and CBV-720, Zeolyst) were used as the Si and/or Al sources. Other starting reagents were the same as those described in refs. [34-37]

[b]Crystallization was performed under rotation (60 or 100 rpm)

40 mA with Ni-filtered Cu K_α X-ray radiation. Elemental analysis involved using a Thermo Scientific iCAP 7400 inductively coupled plasma spectrometer. Crystal morphology and average size were determined by a JEOL JSP-6330F scanning electron microscope (SEM). The N_2 sorption experiments were performed on a Micromeritics ASAP 2020 analyzer.

NH_3 temperature programmed-desorption (TPD) was carried out on a fixed bed, flow-type apparatus linked to a thermal conductivity detector (TCD). A sample of ca. 0.1 g was activated in flowing He (50 mL min^{-1}) at 550 °C for 2 h. Then, 10 wt% NH_3 was passed over the sample at 150 °C for 0.5 h. The treated sample was subsequently purged with He at the same temperature for 1 h to remove physisorbed NH_3. Finally, the TPD was performed in flowing He (30 mL min^{-1}) from 150 to 650 °C at a temperature ramp of 10 °C min^{-1}.

3. Catalysis

The chloromethane conversion was under atmospheric pressure in a continuous-flow apparatus with a stainless steel fixed-bed microreactor (O.D.=1.3 cm, I.D.=1 cm, and length=40 cm). Prior to the experiments, the catalyst was routinely activated under flowing N_2 (10 mL min^{-1}) at 450 °C for 1 h and kept at 400 °C and atmospheric pressure to establish a standard operating procedure, allowing time for the reactant/carrier gas distribution to be stabilized. Then, chloromethane gas (Rigas, 99.9%) was fed at a rate of 2.5 mL min^{-1} (1.73 h^{-1} WHSV) into the reactor, which contained 0.2 g of catalyst, at the same temperature. The total gas flow with N_2 at the reactor inlet was kept constant at 13 mL min^{-1}. The reaction products were analyzed on-line in a Young-Lin YL6100 gas chromatograph (GC) equipped with an HP Plot Q capillary column (30 m× 0.53 mm) and a flame ionization detector. To avoid having the co-produced HCl damage the capillary column, the outlet gas was diluted with He (10 mL min^{-1}) before injection into the GC. Conversion was defined as the percentage of chloromethane consumed during the reaction, and the selectivity of each product was calculated as the percentage amount (in moles) of chloromethane converted to hydrocarbons. Finally, the yield of each product was determined as the multiplication of conversion and selectivity.

RESULTS AND DISCUSSION

1. Physicochemical Properties of Catalysts

Fig. 2 shows the powder XRD patterns of the proton form of all

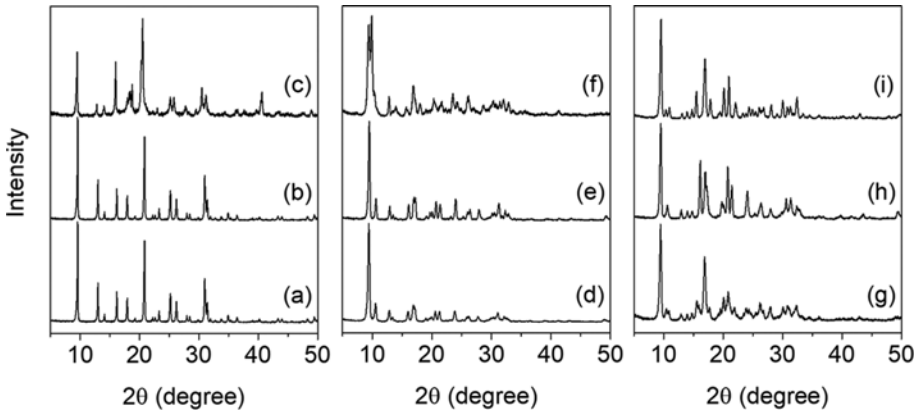

Fig. 2. Powder XRD patterns of proton form (a) H-SAPO-34, (b) H-SSZ-13, (c) H-TiAPSO-34, (d) H-SAPO-18, (e) H-SSZ-39, and (f) H-TiAPO-18 and as-made (g) SAPO-18, (h) SSZ-39, and (i) TiAPO-18.

Table 2. Physicochemical properties of zeolytic catalysts prepared in this study

Catalyst	IZA code	Chemical composition[a]	Crystallite shape and size (μm)[b]	BET surface area (m^2 g^{-1})[c]			Relative acid sites density (a.u.)[e]			
				Total	External[d]	Microporous	Total	Weak	Medium	Strong
H-SAPO-34	CHA	$Si_{0.14}Al_{0.52}P_{0.34}O_2$	Cuboids, <0.2	620	80	540	100	29 (210)	71 (375)	0 (-)
H-SSZ-13	CHA	$Al_{0.07}Si_{0.93}O_2$	Cuboids, <0.7	840	80	760	55	4 (210)	14 (370)	37 (475)
H-TiAPSO-34	CHA	$Ti_{0.01}Si_{0.14}Al_{0.53}P_{0.32}O_2$	Cuboids, <0.2	600	100	500	99	31 (210)	68 (400)	0 (-)
H-SAPO-18	AEI	$Si_{0.07}Al_{0.50}P_{0.43}O_2$	Irregular rods, <0.5	620	100	520	52	22 (210)	30 (345)	0 (-)
H-SSZ-39	AEI	$Al_{0.12}Si_{0.88}O_2$	Cuboids, <1	490	90	400	84	7 (210)	24 (350)	53 (505)
H-TiAPO-18	AEI	$Ti_{0.05}Al_{0.51}P_{0.44}O_2$	Plates, <1	580	70	510	20	20 (210)	0 (-)	0 (-)

[a]Determined by elemental analysis

[b]Determined by SEM

[c]Calculated from N_2 sorption data

[d]Determined according to the *t*-plot method

[e]Determined from peak decomposition of NH_3-TPD data using the PeakFit curve-fitting program. The values given in parentheses are the temperature maxima (°C) of each NH_3 desorption peak

six CHA- and AEI-type zeolytic catalysts employed in this study. For comparison, the XRD patterns of as-made SAPO-18, SSZ-39, and TiAPO-18 are also given in Fig. 2. All the H-form catalysts are highly crystalline and no reflections other than those from each CHA and AEI structure are observed, except for some differences in the H-TiAPO-18 [38]. The highly microporous BET surface areas of all the catalysts were also consistent with their highly crystalline microporous zeolytic structures (Table 2). The rather high external surface areas of the samples may be due to their small crystallite sizes below 1 μm (see below). In our previous study, we confirmed the incorporation of titanium into the tetrahedral framework of TiAPSO-34 and TiAPO-18 by diffuse reflectance infrared Fourier transform and ^{29}Si MAS NMR analyses [34]. Although the relative quantities of titanium are small, i.e., ca. 1 and 5 mol% in H-TiAPSO-34 and H-TiAPO-18, respectively, the tetravalent heteroatom was usually incorporated in the Si and/or P sites of each framework (Table 2).

Interestingly, despite being the same AEI-type of zeolytic materials, the XRD pattern of H-TiAPO-18 is quite different than those of H-SAPO-18 and H-SSZ-39, especially the most intense peaks appeared around 2θ=8.5-11.5°. When compared to the patterns of the as-made materials, on the other hand, the XRD pattern of SSZ-39 is dissimilar to those of SAPO-18 and TiAPO-18. Unlike the patterns of their proton forms, the as-made SAPO-18 and TiAPO-18 are quite similar, although there are some additional peaks in SAPO-18 than TiAPO-18 (e.g., 2θ=15-25°), due to the silicon-rich regions of the structure [36]. Except for some differences in the relative X-ray peak intensities of H-SSZ-39, however, the X-ray peak positions are almost unchanged from its as-made form. It has been reported that unlike the CHA structure, the framework of the AEI-type materials is somewhat flexible, and the unit cell dimensions and T-O-T (T=Al, P, or Si) angles can be changed by calcination, dehydration, rehydration, substitution of framework atoms, etc. [36]. When compared to the AlPO-18 data reported in the literature [36], the XRD patterns of as-made SAPO-18 and TiAPO-18 were found to be similar to that of as-made AlPO-18. The as-made SSZ-39 and the proton forms H-SAPO-18 and H-SSZ-39 are similar to the calcined AlPO-18, whose space group is identical to its as-made form (i.e., *C2/c*), while the detailed unit cell parameters were changed. The unique XRD pattern of H-TiAPO-18, which may be due to the incorporation of titanium in the framework and the resulting change in hydration capability, indicates a more intense structural variation. A systematic investigation which focused on this phenomenon will be discussed in a separate report in the near future. In any case, these structural distortions are rarely observed in zeolite chemistry, but generally tend to influence application properties, i.e., ion-exchange, sorption, catalysis, etc. [39].

Fig. 3 shows SEM images of the six proton form CHA- and AEI-type zeolytic catalysts studied here. The crystallite shapes and sizes of all the catalysts are also summarized in Table 2. There are few changes compared to those of their as-made samples (not shown). The crystallite shapes of all the catalysts are also consistent with the individual conventional crystal morphology [34-37]. We note here that none of the catalysts differed significantly in crystallite size, which ranged from 0.1-1.0 μm. It is well known

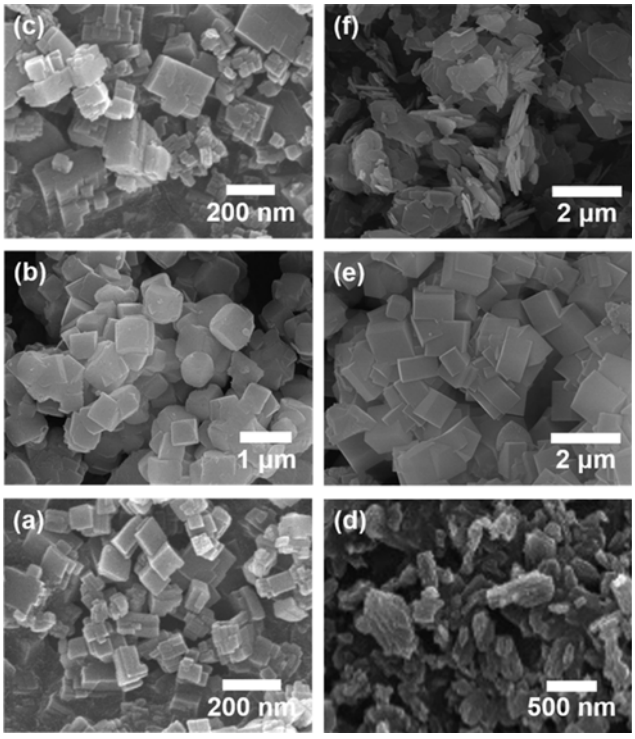

Fig. 3. SEM images of (a) H-SAPO-34, (b) H-SSZ-13, (c) H-TiAPSO-34, (d) H-SAPO-18, (e) H-SSZ-39, and (f) H-TiAPO-18.

that MTO activity is greatly influenced by the catalyst crystal size because of a severe intracrystalline diffusion limitation. For example, when two different H-SAPO-34 catalysts with similar physicochemical properties, but different crystallite sizes (ca. 0.4 vs 7.0 μm), were compared, the smaller crystal H-SAPO-34 catalyst retained a conversion of more than 50% up to 300 min on stream, but under the identical reaction conditions, the larger crystal catalyst rapidly deactivated, and fell below 10% conversion before even 100 min on stream [40]. Therefore, it is important to prepare the catalysts so that they have similar crystal sizes before comparing framework topologies and acidic properties by modifying framework atoms in the CMTO as well as the MTO reaction.

Fig. 4 compares the NH_3 TPD profiles from the six CHA- and AEI-type acid catalysts composed with different framework atoms. Diverse TPD profiles appeared depending on the framework topologies and the composition of the framework atoms. The TPD curves are characterized by one, two, or three desorption peaks with maxima in the temperature regions 200-220, 340-400, and/or 470-510 °C, which are assigned to NH_3 desorption from weak, medium, and strong acid sites, respectively. Their relative area, the relative density, is listed in Table 2. The total relative density of acid sites is strongly proportional to the relative amount of tetrahedrally coordinated framework atoms (Si, Al, Ti+Si, and Ti for H-SAPOs, H-zeolites, H-TiAPSO, and H-TiAPO, respectively) which induce the Brönsted acidity. In a comparison of H-SAPO-34 vs H-SSZ-13 or H-SAPO-18 vs H-SSZ-39, the TPD curves of H-SAPOs consist of weak and medium acid sites, while those of the H-zeolites have considerably higher strong acid sites. This result is very consistent with the general acidic properties of these two group of

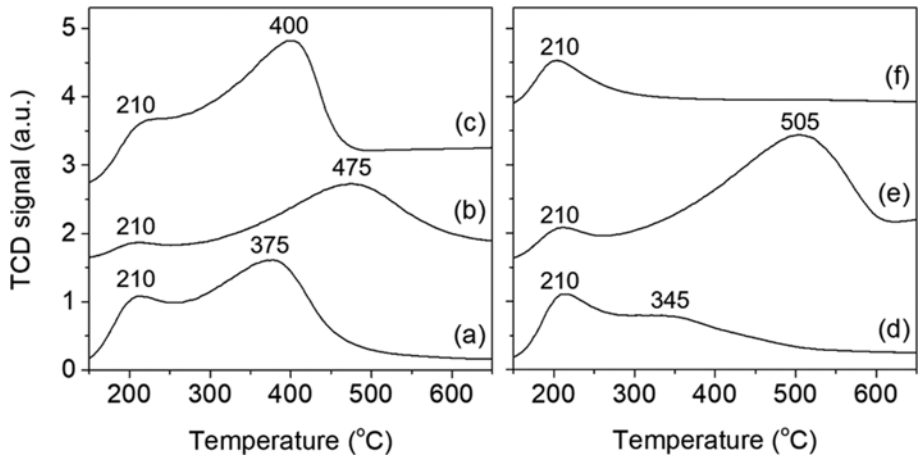

Fig. 4. NH_3 TPD curves of (a) H-SAPO-34, (b) H-SSZ-13, (c) H-TiAPSO-34, (d) H-SAPO-18, (e) H-SSZ-39, and (f) H-TiAPO-18.

zeolytic catalysts [30,36].

Note that the medium acid sites in H-TiAPSO-34 shifted to higher strength (400 vs 375 °C) than in H-SAPO-34, despite having almost the same acid density. This can be rationalized by considering the ^{29}Si MAS NMR results reported in our previous study [34]. The ^{29}Si NMR spectrum of SAPO-34 showed only one strong band around -91 ppm, which corresponds to the Si(4Al) sites. Other small ^{29}Si NMR bands additionally appeared in TiAPSO-34 around –95~

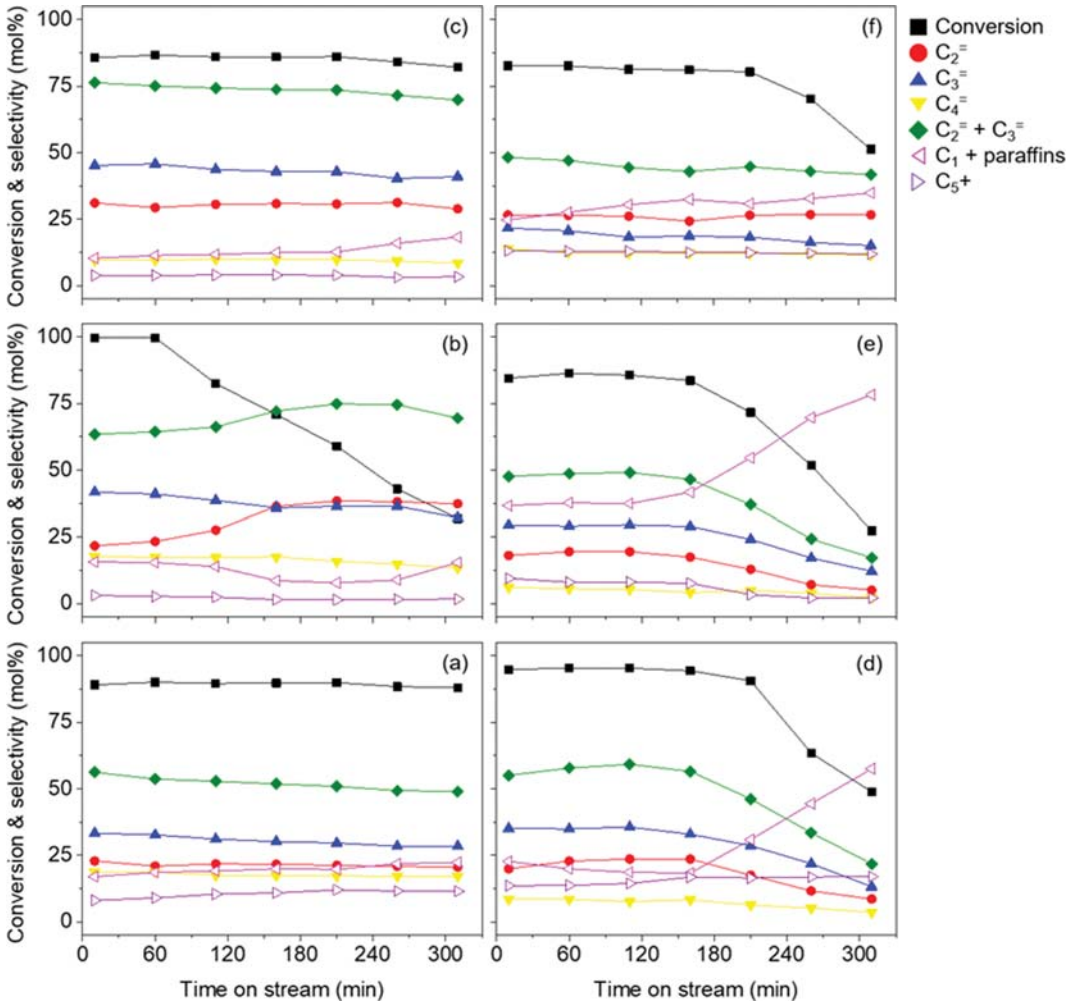

Fig. 5. Conversion of chloromethane and selectivity to hydrocarbons as a function of TOS over (a) H-SAPO-34, (b) H-SSZ-13, (c) H-TiAPSO-34, (d) H-SAPO-18, (e) H-SSZ-39, and (f) H-TiAPO-18 at 400 °C and 1.73 h^{-1} WHSV.

−110 ppm, which can be assigned to Si(nAl) sites (n=0-3). It is known that the Si(nAl) (n=1-3) sites in H-SAPO catalysts usually induce relatively stronger Brönsted acid sites than Si(4Al) sites [15,41]. Thus, the additional incorporation of titanium into the H-SAPO-34 framework gives rise to changes in the acidic property of H-TiAPSO-34. On the other hand, the titanium incorporated H-TiAPO-18 catalyst showed only a weak acid site unlike H-SAPO-18, which has an additional medium acid site. It has been reported that the intensity of higher temperature NH_3 desorption peak increases with increasing Si content in H-SAPO-18 [36]. Thus, a small amount of tetrahedral framework titanium atoms may be responsible for the weak and small amount of acid sites.

2. Chloromethane Conversion Catalysis

Fig. 5 shows the chloromethane conversion and selectivity to hydrocarbons as a function of time on stream (TOS) over all the CHA- (left (a)-(c); H-SAPO-34, H-SSZ-13, and H-TiAPSO-34) and AEI-type (right (d)-(f); H-SAPO-18, H-SSZ-39, and H-TiAPO-18) zeolytic catalysts prepared in this study. We confirmed that all the zeolytic structures were still intact after the entire reaction time, using powder XRD measurements (not shown). We also confirmed that under identical reaction conditions (400 °C and 1.73 h^{-1} WHSV), the methanol conversion remained at almost 100% until around 5 h on stream in the MTO reaction over H-SAPO-34 (not shown). As shown in Fig. 5, on the other hand, except for the H-SSZ-13, none of the catalysts including H-SAPO-34 were able to reach 100% of initial chloromethane conversion after 10 min on stream, despite the relatively high temperature and low WHSV reaction conditions. This result demonstrates that chloromethane has a lower proton affinity than methanol and accordingly lower CMTO reaction activity [5]. We also note that the CMTO kinetic behaviors of all the catalysts studied here showed obvious distinctions, due not only to the framework topologies, but also to the composition of the framework atoms.

2-1. Comparison of the CHA-Type Zeolytic Catalysts

The main reasons for the distinct CMTO kinetic behaviors of the various CHA-type catalysts were their different acidic properties, which had been modified by the different framework atoms, and to a lesser extent, the different catalyst crystal sizes. As shown in Fig. 5(a)-(c), for example, the aluminosilicate H-SSZ-13 with the strong acid sites but with the lowest density of total acid sites had the highest initial conversion (ca. 100%) but its stability, catalyst life time (ca. 120 min), which is defined as the time required to achieve 80% chloromethane conversion, was the shortest among the three CHA-type catalysts. In contrast, H-SAPO-34 and H-TiAPSO-34, with the highest density of total acid sites but without strong acid sites, were characterized by conversions of around 85% during the entire reaction time studied here. The conversion of H-SAPO-34 was slightly higher than that of H-TiAPSO-34, which may be due to the slightly weaker medium acid sites of H-SAPO-34, despite having a similar density of total acid sites. These results indicate that the stronger acid strength has a more negative affect on the catalyst life time than the density of acid sites. It has been known that in the MTO reaction, after the formation of hydrocarbon pool aromatics within most of the zeolite cages, the strong acid sites induce successive cyclization of the aromatics, their progressive growth, and consequently catalyst deactivation [29]. However, this should not rule out the possibility that the slightly larger catalyst crystal size of H-SSZ-13 (ca. 700 vs 200 nm) might also contribute to the faster deactivation [40].

As also shown in Fig. 5(a)-(c), H-SAPO-34 and H-TiAPSO-34 exhibit almost time-independent product selectivity because of their high catalytic stability [26]. However, the product distribution of H-SSZ-13 was changed as a result of catalyst deactivation. Interestingly, despite the almost identical physicochemical properties of H-SAPO-34 and H-TiAPSO-34, e.g., crystallite shape and size, BET surface area, density of total acid sites, etc. as summarized in Table 2, H-TiAPSO-34 exhibited much higher selectivity to light olefins (especially, ethene and propene). The only different physicochemical property between the two CHA-type acid catalysts is the strength of medium acid site: the slightly higher NH_3 desorption peak maximum (400 vs 375 °C) for H-TiAPSO-34 than H-SAPO-34. Although the ethene/propene ratio is similar, 0.64-0.73 and 0.64-0.77 for H-SAPO-34 and H-TiAPSO-34, respectively (the left side of Fig. 6), the selectivity to ethene+propene from H-TiAPSO-34 was ca. 20% higher than that from H-SAPO-34 during the entire reaction time, and therefore remained higher than 70% (Fig. 5(a) and (c)). It thus appears that the increased acid strength in the H-TiAPSO-34, modified by the incorporation of titanium

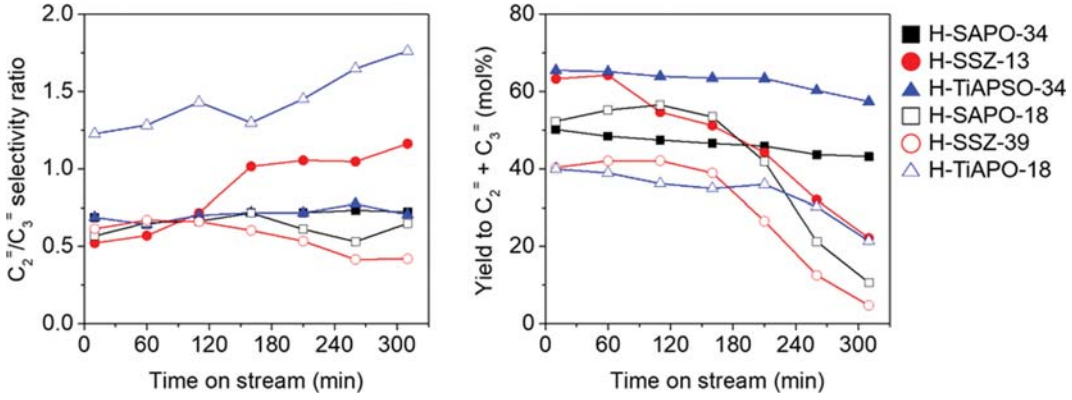

Fig. 6. Relative ratio of $C_2^=$ and $C_3^=$ selectivity (left) and yield to $C_2^=+C_3^=$ (right) as a function of TOS over zeolytic catalysts prepared in this study.

atoms, is associated with a higher selectivity to light olefins. As shown on the right side of Fig. 6, the yield of ethene+propene in the H-TiAPSO-34 remained higher than 60% during the entire reaction time, and it was highest among all the catalysts studied here.

2-2. Comparison of the AEI-type Zeolytic Catalysts

Like the CMTO results for the CHA-type catalysts, the distinct kinetic behaviors of the AEI-type catalysts were also compared based on their different acidic properties. As shown in Fig. 5(d)-(f), H-SAPO-18 with proper acid strength and amount of total acid density, exhibits the highest initial conversion (ca. 95%) and the longest catalyst life time (ca. 230 min) among the three AEI-type catalysts. Similar to the results for H-SSZ-13, the catalytic stability of aluminosilicate H-SSZ-39 is poorer than the other two AEI-type catalysts: ca. 175 min of catalyst life time. This could also be because H-SSZ-39 had the highest density of strong acid sites. This strong acid property of H-SSZ-39 may also be responsible for its relatively low initial conversion. When kinetic behaviors of H-SAPO-18 and H-TiAPO-18 are compared, H-TiAPO-18 with the lowest density of weak acid sites exhibited lower chloromethane conversion and lower catalyst life time. This implies that an appropriate amount of medium acid sites is needed to enhance both initial conversion and stability. Of course, the slightly larger catalyst crystal size of H-TiAPO-18 (ca. 1,000 vs 500 nm) could also lead to a shorter catalyst life time. On the other hand, when compared between H-SSZ-39, which had the highest acid density and strong acid sites, and H-TiAPO-18 with the lowest density and only weak acid sites, although the initial conversions are almost the same: ca. 85 and 83% for H-SSZ-39 and H-TiAPO-18, respectively; the catalytic stability of H-TiAPO-18 (ca. 210 min of catalyst life time) was better than that of H-SSZ-39. It thus also appears that stronger acid strength negatively affects catalyst stability.

As also shown in Fig. 5(d)-(f), among the three AEI-type catalysts, only H-TiAPO-18 exhibits almost time-independent product selectivity even during the period of catalyst deactivation. On the other hand, H-SAPO-18 and H-SSZ-39 show a rapid reduction in product selectivity, including light olefins. The exceptions were methane+paraffins (mainly, ethane), whose selectivity instead increased during the deactivation period. This may have been because the stronger acid sites of these two SAPO and aluminosilicate AEI-type catalysts induced hydrogen transfer to the olefin precursors, and then increased the formation of paraffins simultaneously with the cyclization of hydrocarbon pool aromatics, and then catalyst deactivation [29]. As a consequence, the selectivity to ethene+propene only remained higher than 40% in H-TiAPO-18 during the entire reaction time. Note also that the ethene/propene ratio in H-TiAPO-18 remained higher than one, 1.23-1.76, which was the highest value among all the catalysts studied here (the right side of Fig. 6). However, the relative light olefin ratios of the other two AEI-type catalysts were below one (0.53-0.71 and 0.42-0.67 for H-SAPO-18 and H-SSZ-39, respectively), for the entire reaction time, which will be further discussed below. The details are beyond the scope of this study, but we speculate that one of the possible reasons for the different product shape selectivity of H-TiAPO-18 could be the difference in structure of this titanium incorporated catalyst, as discussed above (Fig. 2).

2-3. Comparison between the CHA- and AEI-type Zeolytic Catalysts

Even when their framework atoms are identical, like SAPO or aluminosilicate, it is not easy to prepare zeolytic catalysts with different framework types that retain almost the same physicochemical properties: the same density and distribution of acid sites, acid strength, crystal size, BET surface area, etc. This makes it difficult to conduct a quantitative comparison of the kinetic behavior of the catalysis over the different framework catalysts. As mentioned, in this study we prepared three pairs of CHA and AEI-type zeolytic catalysts with different framework atoms, (H-SAPO-34 and H-SAPO-18, H-SSZ-13 and H-SSZ-39, and H-TiAPSO-34 and H-TiAPO-18), but of course their respective properties were not the same, as shown in Table 2. Nonetheless, there were some trends in their kinetic behavior, especially in the product selectivity, in the CMTO reaction over these different framework catalysts. As shown on the left side of Fig. 6, for example, the ethene/propene ratio of AEI-type H-SAPO-18 varied between 0.53-0.71 within the overall TOS intervals, which is lower than that (0.64-0.73) of the CHA-type H-SAPO-34. A similar trend can also be observed with H-SSZ-39 and H-SSZ-13: 0.42-0.67 and 0.52-1.16, respectively. This can be explained by the larger volume of the *aei*-cage in the AEI structure. This allowed the hydrocarbon pool transients with the proper size to produce propene to be more stable rather than the smaller sized *cha*-cage in the CHA structure. This relative light olefin selectivity is consistent with the MTO reaction [28,29].

CONCLUSIONS

The CMTO reaction was investigated over CHA-type H-SAPO-34, H-SSZ-13, and H-TiAPSO-34, and also over AEI-type H-SAPO-18, H-SSZ-39, and H-TiAPO-18 at 400 °C, atmospheric pressure, and 1.73 h^{-1} WHSV to compare their kinetic behavior depending on their physicochemical properties, as modified by the compositions of framework atoms and different zeolytic frameworks. It was found that the acidic properties of catalysts with identical framework topology were changed by the inclusion of different framework atoms. Accordingly, the initial conversion and stability, as well as the product selectivity in the CMTO reaction, were directly influenced by the modified acidic properties. In particular, the incorporation of titanium in the H-TiAPSO-34 induced a slightly higher strength of medium acid sites than the counterpart H-SAPO-34, although their total acid densities as well as the other physicochemical properties were almost similar. Due to this small change, H-TiAPSO-34 exhibited slightly lower chloromethane conversion, but ca. 20 mol% higher selectivity to ethene and propene than H-SAPO-34, and therefore showed the best performance among all the catalysts studied here. Furthermore, in comparison with the CHA-type catalysts, the AEI-type catalysts produced relatively more propene than ethene due to the intrinsic larger volume of the *aei*-cage in the AEI structure.

ACKNOWLEDGEMENTS

This work was supported by C1 Gas Refinery Program through the National Research Foundation of Korea (NRF) funded by the

Ministry of Science and ICT (2016M3D3A1A01913251) and the research program of the Korea Institute of Energy Technology Evaluation and Planning (KETEP) funded by Ministry of Trade, Industry & Energy (20153010092090).

REFERENCES

1. R. Horn and R. Schlögl, *Catal. Lett.*, **145**, 23 (2015).
2. P. Tang, Q. Zhu, Z. Wu and D. Ma, *Energy Environ. Sci.*, **7**, 2580 (2014).
3. Y. Wei, D. Zhang, Z. Liu and B.-L. Su, *Chin, J. Catal.*, **33**, 11 (2012).
4. P. Tian, Y. Wei, M. Ye and Z. Liu, *ACS Catal.*, **15**, 1922 (2015).
5. U. Olsbye, O. V. Saure, N. B. Muddada, S. Bordiga, C. Lamberti, M. H. Nilsen, K. P. Lillerud and S. Svelle, *Catal. Today*, **171**, 211 (2011).
6. S. Svelle, S. Aravinthan, M. Bjørgen, K.-P. Lillerud, S. Kolboe, I. M. Dahl and U. Olsbye, *J. Catal.*, **241**, 243 (2006).
7. Y. Wei, D. Zhang, F. Chang, Q. Xia, B.-L. Su and Z. Liu, *Chem. Commun.*, 5999 (2009).
8. D. W. Fickel, K. D. Sabnis, L. Li, N. Kulkarni, L. R. Winger, B. Yan and J. G. Chen, *Appl. Catal. A: Gen.*, **527**, 146 (2016).
9. Y. Sun, S. M. Campbell, J. H. Lunsford, G. E. Lewis, D. Palke and L.-M. Tau, *J. Catal.*, **143**, 32 (1993).
10. T. Xu, Q. Zhang, H. Song and Y. Wang, *J. Catal.*, **295**, 232 (2012).
11. M. Ibáñez, M. Gamero, J. Ruiz-Martínez, B. M. Weckhuysen, A. T. Aguayo, J. Bilbao and P. Castaño, *Catal. Sci. Technol.*, **6**, 296 (2016).
12. N. Li, Y.-Y. Zhang, L. Chen, C.-T. Au and S.-F. Yin, *Micropor. Mesopor. Mater.*, **227**, 76 (2016).
13. Y. Wei, D. Zhang, L. Xu, Z. Liu and B.-L. Su, *Catal. Today*, **106**, 84 (2005).
14. Y. Wei, D. Zhang, Z. Liu and B.-L. Su, *J. Catal.*, **238**, 46 (2006).
15. Y. Wei, Y. He, D. Zhang, L. Xu, S. Meng, Z. Liu and B.-L. Su, *Micropor. Mesopor. Mater.*, **90**, 188 (2006).
16. Y. Wei, D. Zhang, Y. He, L. Xu, Y. Yang, B.-L. Su and Z. Liu, *Catal. Lett.*, **114**, 30 (2007).
17. Y. Wei, D. Zhang, L. Xu, F. Chang, Y. He, S. Meng, B.-L. Su and Z. Liu, *Catal. Today*, **131**, 262 (2008).
18. M. H. Niosen, S. Svelle, S. Aravinthan and U. Olsbye, *Appl. Catal. A: Gen.*, **367**, 23 (2009).
19. A. Zhang, S. Sun, Z. J. A. Komon, N. Osterwalder, S. Gadewar, P. Stoimenov, D. J. Auerbach, G. D. Stucky and E. W. McFarland, *Phys. Chem. Chem. Phys.*, **13**, 2550 (2011).
20. Z. Jiang, B.-X. Shen, J.-G. Zhao, L. Wang, L.-T. Kong and W.-G. Xiao, *Ind. Eng. Chem. Res.*, **54**, 12293 (2015).
21. D. Naumain and B.-L. Su, *Catal. Today*, **73**, 187 (2002).
22. D. Zhang, Y. Wei, L. Xu, A. Du, F. Chang, B.-L. Su and Z. Liu, *Catal. Lett.*, **109**, 97 (2006).
23. T. Xu, H. Song, W. Deng, Q. Zhang and Y. Wang, *Chin. J. Catal.*, **34**, 2047 (2013).
24. L.-T. Kong, B.-X. Shen, J.-G. Zhao and J.-C. Liu, *Ind. Eng. Chem. Res.*, **53**, 16324 (2014).
25. M. Gamero, A. T. Aguayo, A. Ateka, P. Pérez-Uriarte, A. G. Gayubo and J. Bilbao, *Ind. Eng. Chem. Res.*, **54**, 7822 (2015).
26. M. Dusselier, M. A. Deimund, J. E. Schmidt and M. E. Davis, *ACS Catal.*, **5**, 6078 (2015).
27. M. A. Deimund, L. Harrison, J. D. Lunn, Y. Liu, A. Malek, R. Shayib and M. E. Davis, *ACS Catal.*, **6**, 542 (2016).
28. Y. Wang, S.-L. Chen, Y.-J. Jiang, Y.-Q. Cao, F. Chen, W.-K. Chang and Y.-L. Gao, *RSC Adv.*, **6**, 104985 (2016).
29. R. Martínez-Franco, Z. Li, J. Martínez-Triguero, M. Moliner and A. Corma, *Catal. Sci. Technol.*, **6**, 2796 (2016).
30. N. Martin, Z. Li, J. Martínez-Triguero, J. Yu, M. Moliner and A. Corma, *Chem. Commun.*, **52**, 6072 (2016).
31. International Zeolite Association, Structure Commission, http://www.iza-structure.org.
32. L. Xu, Z. Liu, A. Du, Y. Wei and Z. Sun, *Stud. Surf. Sci. Catal.*, **147**, 445 (2004).
33. E. Aghaei, M. Haghighi, Z. Pazhohniya and S. Aghamohannadi, *Micropor. Mesopor. Mater.*, **226**, 331 (2016).
34. H.-J. Chae, S. S. Park, Y. H. Shin and M. B. Park, *Micropor. Mesopor. Mater.*, **259**, 60 (2018).
35. M. Itakura, I. Goto, A. Takahashi, T. Fujitani, Y. Ide, M. Sadakane and T. Sano, *Micropor. Mesopor. Mater.*, **144**, 91 (2011).
36. J. Chen, P. A. Wright, J. M. Thomas, S. Natarajan, L. Marchese, S. M. Bradley, G. Sankar and C. R. A. Catlow, *J. Phys. Chem.*, **98**, 10216 (1994).
37. P. Wagner, Y. Nakagawa, G. S. Lee, M. E. Davis, S. Elomari, R. C. Medrud and S. I. Zones, *J. Am. Chem. Soc.*, **122**, 263 (2000).
38. M. M. J. Treacy and J. B. Higgins, *Collection of Simulated XRD Powder Patterns for Zeolites*, 5th Ed., Elsevier, Amsterdam (2007).
39. M. B. Park, A. Vicente, C. Fernandez and S. B. Hong, *Phys. Chem. Chem. Phys.*, **15**, 7604 (2013).
40. K. Y. Lee, H.-J. Chae, S.-Y. Jeong and G. Seo, *Appl. Catal. A: Gen.*, **369**, 60 (2009).
41. P. P. Man, M. Briend, M. J. Peltre, A. Lamy, P. Beaunier and D. Barthomeuf, *Zeolites*, **11**, 563 (1991).